Development of a Micropyrolyzer for Enhanced Isotope Ratio Measurement

ARTICLE *in* INDUSTRIAL & ENGINEERING CHEMISTRY RESEARCH · OCTOBER 2008

Impact Factor: 2.59 · DOI: 10.1021/ie8009236

Article

Development of a Micropyrolyzer for Enhanced Isotope Ratio Measurement

Jianli Hu, Robert A. Dagle, Bradley R. Johnson, Helen W. Kreuzer, Daniel J. Gaspar, Benjamin Q. Roberts, and M. Lizabeth Alexander

Ind. Eng. Chem. Res., **2008**, 47 (22), 8625-8630 • Publication Date (Web): 24 October 2008

Development of a Micropyrolyzer for Enhanced Isotope Ratio Measurement

Jianli Hu, Robert A. Dagle,* Bradley R. Johnson, Helen W. Kreuzer, Daniel J. Gaspar, Benjamin Q. Roberts, and M. Lizabeth Alexander

Pacific Northwest National Laboratory, 902 Battelle Boulevard, Richland, Washington 99354

This paper presents design, fabrication, and testing of a microscale ceramic reactor for the pyrolysis of organic compounds. One application for this pyrolysis reactor is to convert the oxygen and hydrogen atoms in organic compounds to CO and H_2 for isotope ratio measurements in a continuous flow mode. Existing commercial pyrolyzers use high carrier gas flow rates (typically 80−100 mL/min) such that >95% of the CO and H_2 produced from a given sample is vented before introduction into the mass spectrometer. We describe here the fabrication and testing of a microscale pyrolysis reactor designed to be compatible with existing isotope ratio mass spectrometers. The microreactor uses carrier gas flow rates of 3−5 mL/min, decreasing the proportion of the CO and H_2 lost in venting and permitting analysis of samples 20−50 times smaller than can be analyzed with conventional pyrolysis reactors. Results have shown that organic compounds, such as 1-butanol, ethanol, and ethanolamine, can be fully decomposed to desired products CO and H_2, at a temperature of 1200 °C, which is 200 °C lower than conventionally reported. Furthermore, we are able to eliminate undesired products such as methane and CO_2 in the pyrolysis process. The proof-of-concept experimental results clearly demonstrate that the micropyrolyzer quantitatively converts organic compounds to gases suitable for isotope ratio analysis.

1. Introduction

Stable isotopes are nonradioactive forms of a chemical element with the same chemical properties but different atomic masses. For example, hydrogen exists as ^1H, which is most common, and ^2H, which has one additional neutron and is also known as deuterium. For light elements such as carbon, nitrogen, oxygen, and hydrogen, the most precise method of measuring the isotopic content of a sample is through the use of isotope ratio mass spectrometers. These instruments measure isotopic content with respect to internationally recognized standards and typically report isotopic content in the form of a ratio of the heavy to the light isotope (e.g., $^2H/^1H$). They are capable of high throughput and can distinguish isotopic content that differs by a few to less than one part per thousand (called per mil, or ‰). This scale of difference is observed between various natural samples that are otherwise chemically identical, and therefore, stable isotope ratios can distinguish between chemically identical samples that have not been deliberately labeled. Stable isotope composition thus provides a naturally occurring taggant—the label is permanent as long as the basic molecules in a material remain in their original state.

Stable isotope ratios have demonstrated utility in various areas of biology, including ecology, paleontology, environmental science, and zoology.[1,2] For biological samples, differences in isotopic ratios can arise from organic compounds in the diet of an organism, which are then incorporated into tissues. Therefore, carbon and nitrogen isotope ratios reveal information about food sources and can be used to reconstruct paleodiets and delineate food webs.[3−7] They can also be used to trace isotopically distinct additions, such as nitrogen from agricultural runoff, through ecosystems[8] and to reveal whether pollutants are being actively biodegraded or merely diluted in the environment.[9−13]

The oxygen and hydrogen isotope ratios of tissues reflect both dietary and water inputs and can, thus, act as a recorder of diet and/or drinking water.[14−18] The isotope ratios of surface water are influenced by geography and climate and, thus, vary geographically.[19,20] Isotope ratios of oxygen and hydrogen in tissues such as feathers and wing scales have been used to trace origins and movements of animals and insects between geographical locations where food and/or water differ in their isotope ratios.[21−26] Investigators have now demonstrated that the same relationships apply to human hair.[27−29]

Recently published work suggests that stable oxygen and hydrogen isotope ratios of cellular metabolites may be useful for probing the metabolic rate of microorganisms in various settings. Rapidly growing bacteria derive a large portion of the oxygen and hydrogen atoms in their intracellular water from metabolic activity.[30,31] These atoms become incorporated into cellular metabolites during biosynthesis; thus, the oxygen and hydrogen isotope contents of cellular constituents may record information about the growth rate of the cells at the time of synthesis.

Stable isotope ratios have also been used as a tool in a variety of forensic applications.[32,33] For example, they can serve as a tool for matching samples of materials such as illicit drugs, explosives, toxins, and microbiological agents.[32,34−36] In environmental forensics, isotope ratios of hydrocarbons can associate environmental samples with sources.[9,37−40] Stable isotopes are used to detect adulteration of food and agricultural products[41−47] and can be used to associate microbial cultures with potential culture media and water sources.[36,48,49] Stable isotope analysis has also been suggested as a tool for determining likely regions of origin of unknown human remains.

Many of these applications would be enhanced by reducing the size of samples currently needed for analysis. For example, current instrumentation requires about 150 μg for O and H isotope ratio analysis of solid material such as hair or microbes.[49,50] This amount may seem small, but in fact it means that, for analysis of a single hair (for example), 2.5−3.0 cm is required. This amount represents 2.5−3 months' growth; a smaller sample size offers improved temporal resolution that could provide valuable information on a test subject's movements. Analysis of microbial material, purified metabolites from

* To whom correspondence should be addressed. Tel.: (509) 371-6264. Fax: (509) 376-5106. E-mail: robert.dagle@pnl.gov.

10.1021/ie8009236 CCC: $40.75
Published on Web 10/24/2008

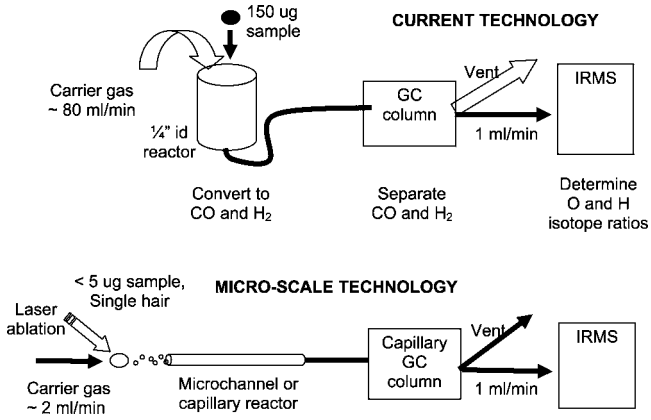

Figure 1. Comparison between conventional isotope ratio analysis and microscale analysis concept.

blood or other body tissues, or traces of explosives would also be greatly facilitated by a reduction in the amount of sample required.

The sample size requirement for isotope ratio analysis of solids is not a function of the isotope ratio mass spectrometer (IRMS) itself. The mass spectrometer of an IRMS instrument is capable of precise isotope ratio measurements of much smaller samples, for example, 20−100 ng of hydrogen.[51] Rather, the limitation is imposed via the means by which the samples are converted to gas (which is required prior to analysis) and introduced into the instrument. For simultaneous analysis of O and H isotope ratios, samples are pyrolyzed in a helium atmosphere under conditions that convert the hydrogen atoms to hydrogen gas and the oxygen into carbon monoxide.[52] These gases are separated chromatographically and enter the mass spectrometer sequentially, where their isotopic content is determined. In currently available instrumentation, the gas stream produced in the initial pyrolysis step is split by a factor of ∼80 before it enters the mass spectrometer, resulting in a loss of nearly 99% of the sample before its introduction into the mass spectrometer.

The ultimate objective of this work is to reduce the amount of solid sample required for analysis by 20−50-fold by building a new device for converting solid samples into CO and H_2, separating them, and introducing them into the IRMS (Figure 1). This report focuses on the design, fabrication, and proof-of-concept demonstration for one component of this device, a micropyrolyzer. Reactor configuration and material selection are discussed. Catalytic and noncatalytic pyrolysis activity performance tests using GC analysis are reported using 1-butanol, ethanol, and ethanolamine as model compounds. Characterization of the coating materials using scanning electron microscope (SEM) is discussed.

2. Experimental Section

Different types of pyrolysis reactors were constructed to evaluate the performance of various coatings and the effect of catalysts on the pyrolysis process. Graphite-coated reactors were prepared using alumina tubes (o.d. = 3 mm, i.d. = 1 mm) approximately 1 m long. The alumina tubes were placed inside a tube furnace where a 6% CH_4/Ar mix was passed through the tube at 1000 °C for 1 h (5 °C/min ramp rate), forming a carbonaceous layer on the alumina subsurface. Boron nitride (BN)-coated pyrolysis reactors were prepared from alumina tubes (o.d = 3 mm, i.d = 1 mm) approximately 1m long. They were coated with a high-purity aqueous suspension of boronitride (BN, Momentive Performance Materials) that contained aluminosilicate binders. The tubes were coated by connecting a 50 mL syringe to the alumina tube using clear, flexible Tygon tubing. The alumina tube was placed in a small bottle containing approximately 20 mL of the BN suspension, and the fluid was suctioned up through the alumina tube by retracting the plunger on the syringe. After drawing up the entire volume of BN suspension, it was then slowly pushed back through the alumina tube using the syringe. This process was repeated two times, then the alumina tube was disconnected from the syringe and turned around, and the above coating process was repeated an additional two times. After suctioning and pushing the BN solution through the alumina tube for a total of four times, the alumina tube was hung vertically and any excess BN suspension was allowed to drain out of the tube. A dry, disposable, laboratory wipe was used to touch the end of the tube to collect any residual solution held inside the bores of the alumina tube by capillary action. Centrifugal force was also used to promote draining of excess BN suspension from the alumina tube. This process was repeated until the interior of the bores on the alumina tube could be visually sighted as being open and free from any BN suspension. The coated alumina tube was then placed on the benchtop and allowed to dry in air. The tube was subsequently calcined at 5 °C/min in air up to 700 °C for 2 h and cooled at the same rate. The coating process was then repeated. After the second coating sequence, the coated alumina tube was calcined at 5 °C/min in air up to 1000 °C.

Both the BN-coated and graphite-coated pyrolysis reactor tubes were then coated with palladium catalyst by a conventional wet impregnation method. Palladium nitrate solution (20% Pd metal) was passed through the reactor in excess. The coated catalyst was then dried at 110 °C for 8 h and calcined at 350 °C (5 °C/min ramp rate) for 3 h. Prior to running activity tests, the catalyst was reduced under 2% H_2/Ar flow at 350 °C for 3 h.

Pyrolysis tests were conducted inside a tube furnace at ambient pressure. A K-type thermocouple was placed near the middle of the reactor as a means to control the furnace temperature. An approximately 20 in. long, high-temperature furnace was used. Graphite-coated, BN-coated, or packed-bed ceramic microchannels were used as microreactors. Graphite-coated and BN-coated tubes were prepared as described above. For the ceramic packed-bed tests, 0.05 g of Pd/Al_2O_3 catalyst was placed in the middle of the 1 mm i.d. ceramic microchannel, kept in place by a quartz wool plug. Otherwise noted, nitrogen was introduced into the system at 5 sccm using a mass flow controller (Brooks 5850E series). Liquid feeds including 1-butanol, ethanol, or ethanolamine were used (Sigma-Aldrich). These liquid feeds are representative of the postlaser ablation particles compounds. Using a syringe pump (Cole Parmer 74900 series), liquid was mixed with the nitrogen prior to entering the reactor fed into a small stainless steel minitube (0.010 in. i.d.) to ensure smooth flow. Unless otherwise noted, liquid was fed via 0.2 mL/h pulses for 3 min. After 3 min, the liquid feed was stopped, and for an additional 7 min, nitrogen purged the system. Gas product was captured in a sample bag continuously for the entire 10 min period. Gaseous effluent contained in the sample bag was analyzed by gas chromatography (MTI model Q30L) equipped with MS-5A and PPQ columns and a thermal conductivity detector (TCD).

Microstructures of the pyrolysis reactors were examined ex situ after completion of all of the reaction experiments. The tubes were filled with epoxy, cured, sectioned into 25 mm long pieces, mounted on end, and recast with epoxy into a cylindrical

mold. The specimens were then polished and examined in a scanning electron microscope (SEM, JEOL 5900) equipped with an energy-dispersive spectrometer (EDS, EDAX Genesis) capable of determining elemental identity of the features of interest. A backscattered electron detector (BSE, Robinson series 8.6) was used for imaging purposes, which provided enhanced contrast based on average atomic number (heavier and denser phases appear brighter).

3. Results and Discussion

3.1. Material Selection and Design Criterion of Micropyrolyzer. The isotope ratio measurement system for which our micropyrolyzer was designed is shown schematically in Figure 1. The system includes three major components: (i) a laser ablation device that converts a trace amount of solid sample into submicron size particles that can be quantitatively transferred into the next component, (ii) the micropyrolyzer, and (iii) an existing isotope ratio mass spectrometer (IRMS). The particles produced via laser ablation are introduced into the microchannel pyrolyzer by carrier gas in a continuous flow mode, where they are pyrolyzed either thermally or catalytically to CO, CO_2, H_2, and CH_4. For isotope ratio analysis, the desired products are CO and H_2, whereas undesired CO_2 and CH_4 must be eliminated. Once CHNO-containing compounds are pyrolyzed into CO, H_2, and N_2, the product gases are separated by gas chromatography (GC) and then fed into the IRMS for isotope ratio analysis. The reactor design ensures plug flow to facilitate downstream IRMS analysis, and the same carrier gas stream carries the product gases into the IRMS. One of the objectives of our reactor design is to achieve 100% pyrolysis efficiency at the lowest possible temperature to minimize insulation and system constraints.

In order to ensure complete pyrolysis of CHNO-containing compounds, reactors are conventionally operated at temperatures up to 1450 °C.[53] At such high temperatures, most metals or alloys cannot be used as materials for reactor fabrication because they either melt or their external surface is oxidized, causing material degradation. Alloy materials that can be operated at high temperature pose a significant fabrication and cost challenge. Metal oxides could be considered for use in pyrolyzer fabrication; however, at such a high temperature, most metal oxides release oxygen that could interfere with the isotopic analysis, even at very low partial pressure. For a metal oxide to be selected, it must have negligible partial pressure, as indicated in the "Ellingham Diagram for Metallurgically Important Oxides".[54] Metal oxides that meet this requirement include MgO, SiO_2, and Mullite. Another candidate material that would not interfere with O and H isotope ratio analysis is boron nitride (BN), which is thermally stable up to 3000 °C and structurally does not contain O or H. In this study, a technique was developed to coat a thin layer of graphite or BN on ceramic capillary tubes. This thin coating on the metal oxide surface (a few microns thick) is expected to prevent the release of oxygen from the metal oxide surface.

3.2. Catalytic Pyrolysis of 1-Butanol. 1-Butanol ($C_4H_{10}O$) was chosen as a model compound feed for the pyrolysis. The effects of thermal pyrolysis were compared to catalytic pyrolysis in a microchannel reactor. As shown in Figure 2, for thermal pyrolysis even when the temperature was increased to 1200 °C, undesired compounds of CO_2 and CH_4 were still observed. When the temperature was further increased to 1450 °C, methane was fully pyrolyzed whereas a trace amount of CO_2 was still observed. To eliminate CO_2 formation, the reactor was then packed with a powder Pd catalyst, known to be active as an alcohol decomposition catalyst. With the catalyst, CO_2 is eliminated even at 1100 °C, as shown in Figure 3. It is likely that CO_2 was reduced via the reaction of $C + CO_2 \rightarrow 2CO$ in the presence of the catalyst. However, at temperatures up to 1200 °C, the Pd catalyst in the packed-bed mode was not able to completely eliminate CH_4. These results suggest that the use of an effective catalyst having a high surface area and enhanced activity can eliminate both CH_4 and CO_2 at temperatures lower than 1450 °C.

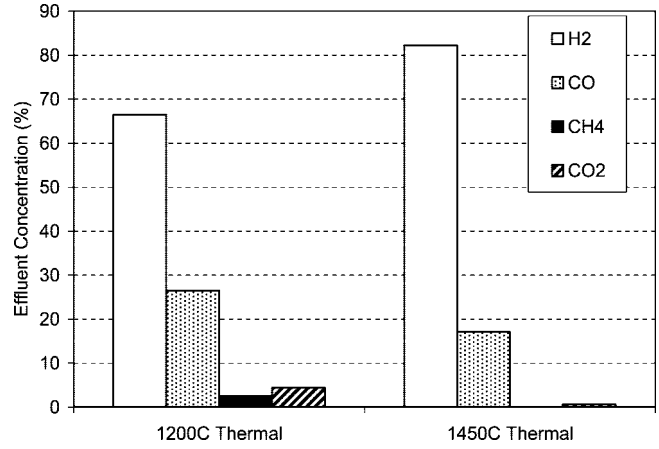

Figure 2. Thermal pyrolysis tests for 1-butanol in a microscale reactor; effluent concentrations via GC analysis versus reaction temperature.

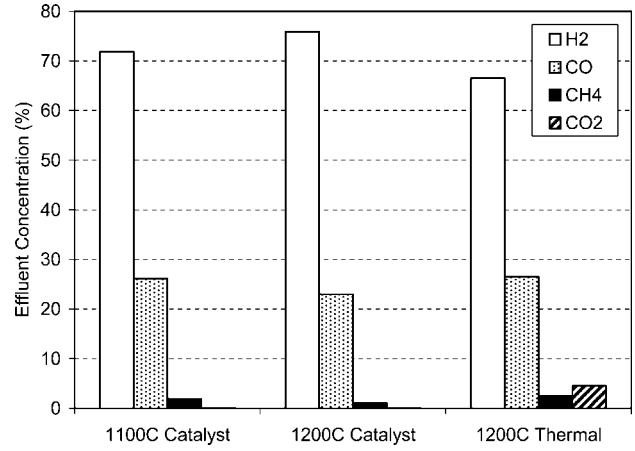

Figure 3. Thermal pyrolysis and packed-bed catalytic pyrolysis for 1-butanol in a microscale reactor; effluent concentrations via GC analysis versus reaction temperature.

Further experiments were carried out using ceramic tubes coated either with graphite or boron nitride (BN). Each type of capillary tube was also coated with Pd catalyst, in order to test catalyzed and uncatalyzed reactions in tubes coated with both materials. Wall coating with catalyst offers less pressure drop while enhancing thermal contact. Furthermore, by using a small microchannel inner diameter (1 mm), diffusion resistances are minimized. As shown in Figure 4, pyrolysis of 1-butanol was carried out in the temperature range 1000−1450 °C, where temperature is plotted against the CH_4/CO ratio. Instead of quantifying the absolute value of CH_4 concentration, the relative concentration of CH_4/CO (mol/mol) was monitored throughout the test. From Figure 4, it is shown that, catalytically, with both the BN and graphite-coated tubes, CH_4 can be fully pyrolyzed at ~1200 °C. CO_2 is catalytically eliminated for the entire temperature range investigated (not shown). In the absence of catalyst, CH_4 can only be fully pyrolyzed at 1450 °C.

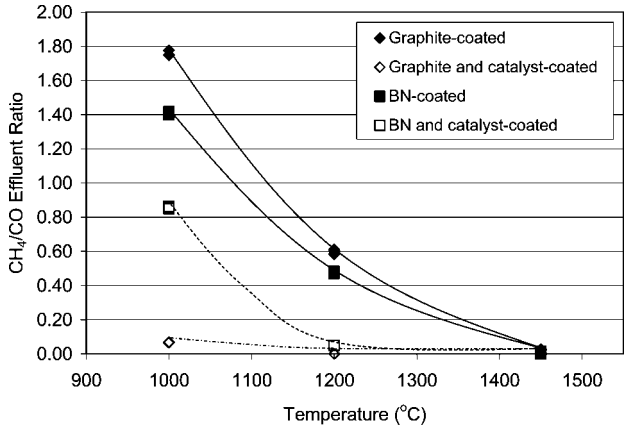

Figure 4. Effect of catalyst on 1-butanol pyrolysis. Graphite and BN-coated tubes with and without catalyst coating were used for comparison; effluent CH_4/CO ratio is shown versus reaction temperature.

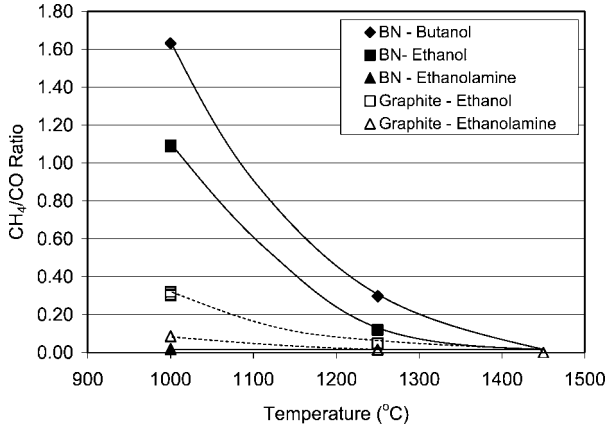

Figure 5. Effect of model feed compound on pyrolysis for 1-butanol, ethanol, and ethanolamine. Graphite and BN-coated microchannels with catalyst coating were used for comparison; effluent CH_4/CO ratio is shown versus reaction temperature.

3.3. Pyrolysis of Ethanol and Ethanolamine. Further experiments were carried out using ethanol (CH_3CH_2OH) and ethanolamine (C_2H_7NO) as model compounds. These two compounds were selected to study the effect of the C/O feed ratio and the presence of a C−N bond on the pyrolysis efficiency. Pyrolysis of 1-butanol indicated that the use of a catalyst allowed for lower-temperature operation. The following experiments were carried out using BN- and graphite-coated channels both coated with a Pd catalyst. As shown in Figure 5, when ethanolamine was used as a feed, the CH_4/CO ratio drops to zero at 1000 °C with the Pd + BN-coated tube and at 1250 °C with the Pd + graphite coated tube. When ethanol was used, the CH_4/CO ratio dropped to zero at 1250 °C rather than 1000 °C. Throughout the entire test, the undesired compounds CO_2 and NH_3 were not detected.

To facilitate future reactor design, the effect of contact time on pyrolysis was investigated. These experiments were carried out at 1000 °C, at which temperature incomplete pyrolysis was expected. This ensured contact time-dependent differences could be observed. As shown in Figure 6, the pyrolysis efficiency is strongly affected by the contact time. CH_4/CO ratio decreased linearly with an increase in contact time. These results indicate that the reactor design should consider longer residence time or higher temperature or should employ more active catalyst to ensure complete pyrolysis of more complex or challenging organic compounds.

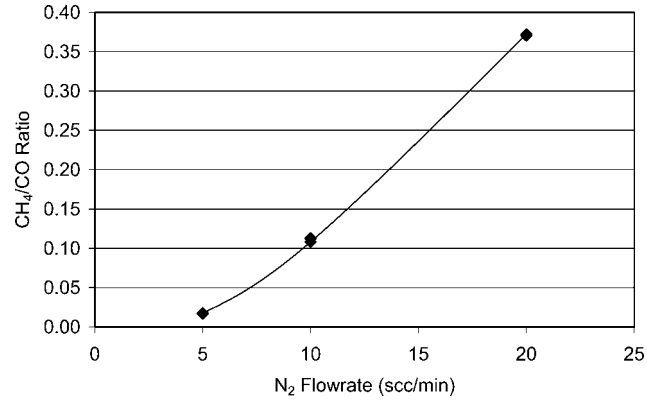

Figure 6. Effect of contact time on catalytic ethanolamine pyrolysis (feed = ethanolamine, temperature = 1000 °C, BN and catalyst-coated microchannel); effluent CH_4/CO ratio shown versus nitrogen feed.

These promising results suggests coated microcapillary tubes provide a controlled means to make an economically feasible micropyrolyzer with the ability to process samples of much smaller size than conventionally utilized. This confirms complimentary earlier work by Burgoyne et al. who demonstrated, for similar applications, full thermal pyrolysis of propane at temperatures above 1430 °C using graphitized alumina tubes.[53] However, by use of a catalyst, the operating temperature can be significantly minimized and/or the rate of reaction can be greatly enhanced. A higher rate of reaction offers reactor size savings, which is a key performance metric for portable applications.

Potential drawbacks imposed by using a catalyst are still a concern. Such potential problems include the following:

(1) Formation of carbon deposits that could inhibit catalytic activity. For example, carbon deposits can be formed on the catalyst through the methane decomposition reaction, $CH_4 \rightarrow C + 2H_2$. Pd-type catalysts are known to be susceptible to hydrocarbon decomposition. Thus, it is likely that some degree of decomposition is occurring. However, decomposition does not affect the isotopic ratio analysis directly. H_2 formation through decomposition still yields H in molecular form, maintaining H isotopic homogeneity. Rather, a potential problem is stability of the catalyst over extended periods during which all, or enough to become problematic, surface sites might be converted to carbon. While only relatively small amounts of material will be "pulsed" over the catalyst, long-term stability of the catalyst will be addressed in subsequent work. If long-term longevity of the system were deemed unacceptable due to coking deposition, different reactor systems could be introduced (i.e., larger reactors or those with higher loadings of catalytic active sites) or regeneration schemes could be enacted. For example, it might be possible to periodically pulse the catalytic reactor with air, thus burning off the carbon.

(2) Oxide formation on the metal catalyst that could affect the O isotopic measurement. This issue will also be addressed in a latter phase of this work, which will integrate the IRMS with the pyrolyzer and validate isotopic ratio analysis.

It should be noted that the model feeds chosen for the pyrolysis reactor evaluation do not *precisely* represent actual feed compounds. In the actual application, the sample will first be converted to submicron size particles by laser ablation and then transferred into the microreactor. Our model *liquid* feed compounds 1-butanol, ethanolamine, and ethanol were chosen with the intent to demonstrate that CHO- and CHNO-containing compounds could by completely pyrolyzed (to CO and H_2). Additionally, under these pyrolysis reaction conditions, non-

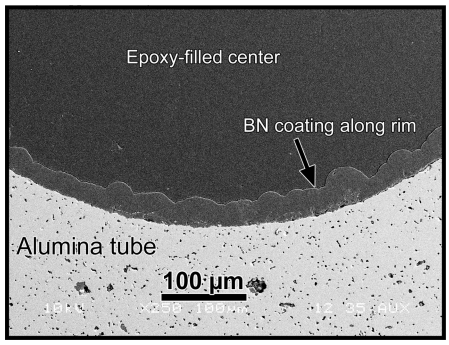

Figure 7. SEM micrograph of the cross section from the BN-coated alumina tube, without catalyst, approximately 7.5 cm from the end of the inlet of the tube.

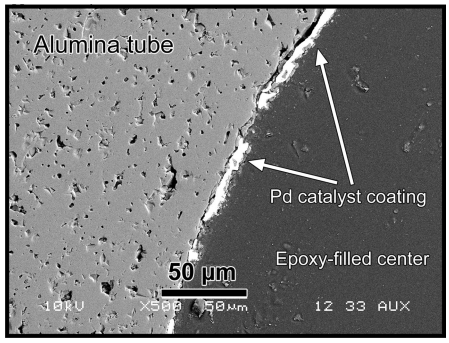

Figure 8. SEM micrograph of the cross section from the BN-coated alumina tube, with catalyst, approximately 30 cm from the end of the inlet of the tube. The white areas are the Pd catalyst.

oxygen-containing materials were evaluated. However, these model compounds do not necessarily mimic the exact characteristics of the *solid* submicron particles exiting the laser ablation. The implications of the mass transport differences between the model liquid feed compounds and the actual submicron particle feed is not yet known. Effectiveness of the heterogeneous catalyst for this particular situation is unclear. Coupling the laser ablation and pyrolysis reaction in subsequent work will address laser ablation efficiency and pyrolysis reaction using postlaser ablation submicron particles.

3.4. Microscopy Characterization of Graphite and BN Coating. SEM analysis of the BN-coated tube revealed several important features. First, the coating process was able to deposit a coating that was approximately 29 μm thick, as shown in Figure 7. The coating was present toward the inlet of the tube, on the nonflow bore of the double-bored alumina tube, but was not located on the bore used for the reactions or on any sections >15 cm from the inlet, shown in Figure 8. Apparently, some combination of high temperatures, high gas flow rates, and/or oxidation caused the BN coating to be completely eliminated. The Pd catalyst coating, however, remained and is easily identified along the interior wall of the bore. Because of its high density and high atomic number, it appeared white using BSE imaging in the SEM, shown in Figure 8. The catalyst coating was not uniform but existed as discrete patches up to 50 μm wide and 5 μm thick (length was measured in cross section). There were many gaps in the catalytic coating along the perimeter of the bore.

Analysis of the graphitic-coated tube also showed some important features. Similar to the BN-coated tube, the coating was nonuniform along the length of the bore. However, the coating improved in quality the closer it was toward the furnace hot zone. Toward the entrance of the tube, only a very thin

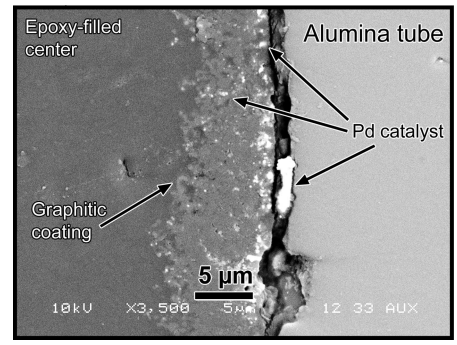

Figure 9. SEM micrograph of the cross section of the graphite-coated alumina tube, with catalyst, approximately 38 cm from the end of the inlet section. The textured light-gray region along the interior of the alumina tube was the graphitic coating, and the white speckles were the Pd catalyst.

coating was observed, which was barely distinguishable from the epoxy used to fill the bore. At approximately 28 cm from the entrance of the tube, the coating was still nonuniform, it had a discontinuous nodular appearance, and it was up to 7−10 μm thick. An important, microstructural change occurred in the graphitic coating at approximately 38 cm from the inlet, which was near the hottest area of the furnace. The coating changed from being irregular, discrete nodules to a finer, more continuous, possibly filamentous coating. This can be seen in Figure 9. The left side (dark gray) of the micrograph is the epoxy-filled bore center. The light gray region on the right side is the alumina wall. The textured, medium gray region toward the central part of the micrograph is the graphitic coating. The benefit of this microstructure is that it appears to have a filamentous texture and would, thus, have a higher surface area. A higher surface area can result in improved catalyst dispersion and subsequently enhanced catalytic activity. Close examination of the graphitic coating in Figure 9 shows that it is covered with white speckles, which are the Pd catalyst.

Proof for the improved microstructure for the graphitized material, leading to improved catalyst dispersion and improved catalytic performance, is seen in Figure 4. Pyrolysis of 1-butanol was enhanced by approximately 40% at 1000 °C by catalytically treating the BN tube; however, there was over a 20-fold improvement in pyrolysis performance (based on CH_4/CO ratio) for the catalytically treated graphitic coated tube. The explanation for the drastically improved performance can be attributed to the higher surface area graphitic coating that yielded an improved catalytic dispersion and enhanced catalytic performance.

The graphitic coating proved more advantageous than the BN coating because it remained attached to the walls of the alumina tube, had a higher surface area, and thus improved catalytic performance of the pyrolysis reactor. Complete disappearance of the BN coating defeats the original intent for providing an oxygen barrier between the alumina oxide surface and the pyrolysis reaction. Thus, coating of the alumina surface with graphite has proven to be a viable option, whereas coating with BN is not. Evaluation of the graphite-coated alumina reactor for maintaining isotopic fidelity of the analyte needs to be confirmed with IRMS.

4. Conclusion

A micropyrolyzer has been developed using a method consisting of coating a ceramic capillary tube with either graphite or boronitride (BN), followed by a catalyst. A proof-of-principle experiment has shown that organic compounds

containing the elements C, H, N, and O can be fully pyrolyzed to the desired products CO and H_2. The undesired products CH_4 and CO_2 can be eliminated by a combination of catalysis, temperature, and residence time. In the presence of catalyst, pyrolysis can be carried out at much lower temperature than in uncatalyzed reactors. The ratio of CO/H_2 and the presence of C−N bonding in the feed do not affect pyrolysis efficiency. SEM characterization indicates the graphite coating maintained its microstructural integrity and provided catalytic surface area enhancement. However, the BN coating was eliminated during reaction. The flow rate of the pyrolysis reactor has been reduced to less than the 5 mL/min required by IRMS. The next phase in the development of this system is to integrate the micropyrolyzer component with an IRMS to validate the isotope ratio analysis.

Acknowledgment

A portion of this work was performed in the Environmental Molecular Sciences Laboratory, a national scientific user facility sponsored by the U.S. Department of Energy's Office of Biological and Environmental Research, located at Pacific Northwest National Laboratory in Richland, WA. We greatly acknowledge funding provided under the Laboratory Directed Research and Development program at Pacific Northwest National Laboratory.

Literature Cited

(1) Fry, B. *Stable Isotope Ecology*; Springer: New York, 2006.
(2) *Stable Isotopes in Ecology and Environmental Science*; Lajtha, K., Michener, R. H. , Eds.; Blackwell Scientific Publications: Cambridge, U.K., 1994.
(3) Schoeninger, M. J.; DeNiro, M. J. *Geochim. Cosmochim. Acta* **1984**, *48*, 625–639.
(4) Fry, B.; Scherr, E. B. *Contrib. Mar. Sci.* **1984**, *27*, 13–47.
(5) DeNiro, M.; Epstein, S. *Geochim. Cosmochim. Acta* **1978**, *42*, 495–506.
(6) DeNiro, M.; Epstein, S. *Geochim. Cosmochim. Acta* **1981**, *45*, 341–351.
(7) Schoeninger, M. J.; DeNiro, M. J.; Tauber, H. *Science* **1983**, *220*, 1381–1383.
(8) Wayland, M.; Hobson, K. A. *Can. J. Zool.* **2001**, *79*, 5–15.
(9) Pond, K. L.; Huang, Y. S.; Wang, Y.; Kulpa, C. F. *Environ. Sci. Technol.* **2002**, *36*, 724–728.
(10) Hunkeler, D.; Aravena, R.; Berry-Spark, K.; Cox, E. *Environ. Sci. Technol.* **2005**, *39*, 5975–5981.
(11) Kirtland, B. C.; Aelion, C. M.; Stone, P. A.; Hunkeler, D. *Environ. Sci. Technol.* **2003**, *37*, 4205–4212.
(12) Lollar, B. S.; Slater, G. F.; Ahad, J.; Sleep, B.; Spivack, J.; Brennan, M.; MacKenzie, P. *Org. Geochem.* **1999**, *30*, 813–820.
(13) Ward, J. A. M.; Ahad, J. M. E.; Lacrampe-Couloume, G.; Slater, G. F.; Edwards, E. A.; Lollar, B. S. *Environ. Sci. Technol.* **2000**, *34*, 4577–4581.
(14) Luz, B.; Kolodny, Y.; Horowitz, M. *Geochim. Cosmochim. Acta* **1984**, *48*, 1689–1693.
(15) Estep, M. *Science* **1981**, *214*, 1374–1376.
(16) Estep, M.; Dabrowski, H. *Science* **1980**, *209*, 1537–1538.
(17) Longinelli, A. *Geochim. Cosmochim. Acta* **1984**, *48*, 385–390.
(18) Hobson, K. A.; Atwell, L.; Wassenaar, L. I. *Proc. Natl. Acad. Sci. U.S.A.* **1999**, *96*, 8003–8006.
(19) Kendall, C.; Coplen, T. B. *Hydrol. Processes* **2001**, *15*, 1363–1393.
(20) Dutton, A.; Wilkinson, B. H.; Welker, J. M.; Bowen, G. J.; Lohmann, K. C. *Hydrol. Processes* **2005**, *19*, 4121–4146.
(21) Braune, B. M.; Hobson, K. A.; Malone, B. J. *Sci. Total Environ.* **2005**, *346*, 156–168.
(22) Chamberlain, C.; Blum, J.; Holmes, R.; Feng, X.; Sherry, T.; Graves, G. *Oecologia* **1997**, *109*, 132–141.
(23) Hobson, K. A. *Oecologia* **1999**, *120*, 314–326.
(24) Hobson, K. A.; Bowen, G. J.; Wassenaar, L. I.; Ferrand, Y.; Lormee, H. *Oecologia* **2004**, *141*, 477–488.
(25) Hobson, K. A.; Wassenaar, L. I. *Oecologia* **1997**, *109*, 142–148.
(26) Hobson, K. A.; Wassenaar, L. I.; Taylor, O. R. *Oecologia* **1999**, *120*, 397–404.
(27) Sharp, Z. D.; Atudorei, V.; Panarello, H. O.; Fernandez, J.; Douthitt, C. *J. Archaeol. Sci.* **2003**, *30*, 1–8.
(28) Fraser, I.; Meier-Augenstein, W.; Kalin, R. M. *Rapid Commun. Mass Spectrom.* **2006**, *20*, 1109–1116.
(29) O'Brien, D.; Wooller, M. *Rapid Commun. Mass Spectrom.* **2007**, *21*, 2422–2430.
(30) Kreuzer-Martin, H. W.; Ehleringer, J. R.; Hegg, E. L. *Proc. Natl. Acad. Sci. U.S.A.* **2005**, *102*, 17337–17341.
(31) Kreuzer-Martin, H. W.; Lott, M. J.; Ehleringer, J. R.; Hegg, E. L. *Biochemistry* **2006**, *45*, 13622–13630.
(32) Benson, S.; Lennard, C.; Maynard, P.; Roux, C. *Forensic Sci. Int.* **2006**, *157*, 1–22.
(33) Slater, G. F. *Environ. Forensics* **2003**, *4*, 13–23.
(34) Casale, J. F.; Ehleringer, J. R.; Morello, D. R.; Lott, M. J. *J. Forensic Sci.* **2005**, *50*, 1315–1321.
(35) Serra, F.; Reniero, F.; Guillou, C. G.; Moreno, J. M.; Marinas, J. M.; Vanhaecke, F. *Rapid Commun. Mass Spectrom.* **2005**, *19*, 1227–1230.
(36) Kreuzer-Martin, H. W.; Jarman, K. *Appl. Environ. Microbiol.* **2007**, *73*, 3896–3908.
(37) Hough, R. L.; Whittaker, M.; Fallick, A. E.; Preston, T.; Farmer, J. G.; Pollard, S. J. T. *Environ. Pollut.* **2006**, *143*, 489–498.
(38) Seki, O.; Yoshikawa, C.; Nakatsuka, T.; Kawamura, K.; Wakatsuchi, M. *Deep-Sea Res., Part I* **2006**, *53*, 253–270.
(39) Kim, M.; Kennicutt, M. C.; Qian, Y. R. *Mar. Pollut. Bull.* **2006**, *52*, 1585–1590.
(40) Andersen, N.; Schoell, M.; Carlson, R. M. K.; Schaeffer, P.; Albrecht, P.; Bernasconi, S. M.; Paul, H. A.; Klaas, C.; Hunkeler, D. *Abstr. Pap. ACS* **2001**, *222*, U485−U485.
(41) Lin, G. P.; Rau, Y. H.; Chen, Y. F.; Chou, C. C.; Fu, W. G. *J. Food Sci.* **2003**, *68*, 2192–2195.
(42) Martinelli, L. A.; Moreira, M. Z.; Ometto, J.; Alcarde, A. R.; Rizzon, L. A.; Stange, E.; Ehleringer, J. R. *J. Agric. Food Chem.* **2003**, *51*, 2625–2631.
(43) Nhu-Trang, T. T.; Casabianca, H.; Grenier-Loustalot, M. F. *Anal. Bioanal. Chem.* **2006**, *386*, 2141–2152.
(44) Ogrinc, N.; Kosir, I. J.; Spangenberg, J. E.; Kidric, J. *Anal. Bioanal. Chem.* **2003**, *376*, 424–430.
(45) Stocker, A.; Rossmann, A.; Kettrup, A.; Bengsch, E. *Rapid Commun. Mass Spectrom.* **2006**, *20*, 181–184.
(46) Tremblay, P.; Paquin, R. *J. Agric. Food Chem.* **2007**, *55*, 197–203.
(47) Versini, G.; Camin, F.; Ramponi, M.; Dellacassa, E. *Anal. Chim. Acta* **2006**, *563*, 325–330.
(48) Kreuzer-Martin, H. W.; Lott, M. J.; Dorigan, J. V.; Ehleringer, J. R. *Proc. Natl. Acad. Sci. U.S.A.* **2003**, 815–819.
(49) Kreuzer-Martin, H. W.; Chesson, L. A.; Lott, M. J.; Dorigan, J. V.; Ehleringer, J. R. *J. Forensic Sci.* **2004**, 49.
(50) Bowen, G. J.; Chesson, L.; Nielson, K.; Cerling, T. E.; Ehleringer, J. R. *Rapid Commun. Mass Spectrom.* **2005**, *19*, 2371–2378.
(51) Sessions, A. L.; Burgoyne, T. W.; Schimmelmann, A.; Hayes, J. M. *Org. Geochem.* **1999**, 30.
(52) Gehre, M.; Strauch, G. *Rapid Commun. Mass Spectrom.* **2003**, *17*, 1497–1503.
(53) Burgoyne, T. W.; Jaynes, J. M. *Anal. Chem.* **1998**, *70*, 5136–5141.
(54) Gaskell, D. R. *Introduction to Metallurgical Thermodynamics*, 2nd ed.; Hemisphere Publishing Corporation: New York, 1981.

Received for review June 11, 2008
Revised manuscript received September 9, 2008
Accepted September 18, 2008

IE8009236